

# Communication-Aware Robot Execution for Cloud Inference under Spatially Heterogeneous Connectivity

Fengkai Liu<sup>✉</sup>, *Student Member, IEEE*, Yuichi Ohsita<sup>✉</sup>, *Member, IEEE*,  
Masayuki Murata<sup>✉</sup>, *Life Member, IEEE*, and Hideyuki Shimonishi<sup>✉</sup>, *Member, IEEE*

arXiv:2606.31497v1 [cs.RO] 30 Jun 2026

**Abstract**—Cloud-hosted foundation models enable robots to use semantic reasoning beyond onboard computational limits. In this setting, the robot executes a currently available primitive generated by the cloud, and continued task progress requires the next cloud result before this primitive is exhausted. This execution becomes fragile under spatially heterogeneous connectivity, because the current primitive determines when the next result is needed, whereas the wireless environment determines where the next request can be submitted and where the response can be retrieved. Strategies that reduce latency or improve individual transmissions can shorten this dependency, but they do not determine a submission location that supports reliable upload and leaves a feasible opportunity for response retrieval. To address this problem, we introduce the request–response window, which characterizes the time required for the next cloud cycle, including uplink transmission, cloud inference, downlink retrieval, and inference uncertainty. Building on this window and an available communication map, the proposed framework treats the next request point as a motion decision during ongoing primitive execution, selecting it to provide sufficient communication quality for cloud request submission while preserving progress within the finite support of the current primitive. The selected request point is incorporated into a local planner, which guides the robot toward the request point before submission and then continues task execution while maintaining sufficient connectivity for retrieving the next cloud result. Experiments in an indoor wireless scenario built from measurements show that the proposed method achieves the best or tied-best task success among the compared methods, while using fewer request attempts and producing lower request failure rates. These results suggest that, in the considered spatially heterogeneous wireless setting, the proposed method helps maintain robot execution under spatially varying connectivity.

**Index Terms**—Cloud robotics, foundation models, mobile robots, wireless communication, path planning.

## I. INTRODUCTION

Large foundation models are reshaping robot autonomy in open environments. Alongside end-to-end Vision-Language-Action (VLA) policies [1]–[3], modular systems use large language or vision language models for semantic guidance while retaining onboard perception, control, and safety critical

This work was supported by JSPS KAKENHI, Grant Number JP25H01118, and by JST SPRING, Grant Number JPMJSP2138.

Fengkai Liu and Masayuki Murata are with Graduate School of Information Science and Technology, The University of Osaka, Osaka, 565-0871, Japan (e-mail: f-liu@ist.osaka-u.ac.jp, murata@ist.osaka-u.ac.jp).

Yuichi Ohsita is with D3 Center, The University of Osaka, Osaka, 560-0043, Japan (e-mail: yuichi.ohsita.cmc@osaka-u.ac.jp).

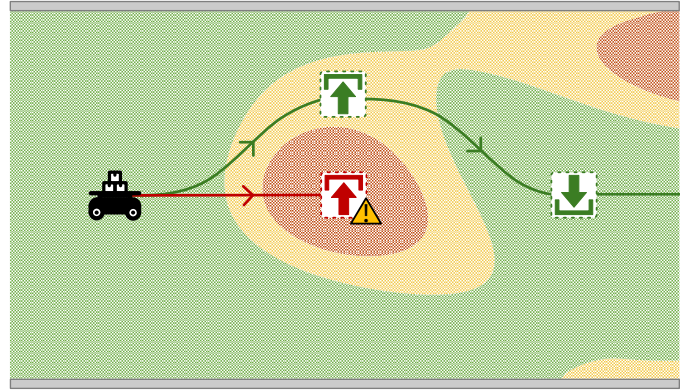


Fig. 1. Motivation of communication-aware request placement. The background indicates spatially varying connectivity, where weak-connectivity regions can make a nominal request candidate unsuitable for submission or response retrieval. The objective is to select a favorable request point and maintain sufficient connectivity over the request–response window until the cloud response is retrieved.

execution [4]. The modular design is particularly attractive when robots need access to powerful models hosted in the cloud despite limited onboard compute [5], [6]. In such systems, the foundation model returns a high-level semantic primitive that is grounded locally into a motion target [7]–[12]. Since this primitive provides only a finite execution horizon, maintaining uninterrupted task progress requires the next primitive to become available before the current one is exhausted. The robot executes the current primitive while the next cloud inference request may be processed asynchronously, as in related asynchronous VLA systems [13]–[15], but sustained execution still depends on whether the next request–response cycle finishes in time. Under unstable connectivity, this dependency becomes fragile [4], [16]: task execution determines when the next result is needed, while network availability during execution may vary with the robot’s location.

Existing mitigation strategies do not fully resolve this problem. Methods such as allocating or replicating cloud service resources and using redundant network paths can reduce average latency or improve the reliability of individual transmissions [17]–[20]. However, they do not determine where the robot should move under spatially varying connectivity. When cloud inference takes long enough for the robot to move substantially before the response returns, the robot’s locations

at both request submission and response retrieval become critical. The robot may still fail if either request submission or response retrieval occurs in a weak-connectivity region, as illustrated in Fig. 1. This problem therefore couples robot motion, spatially varying connectivity, and cloud inference latency during execution. The key requirement is to reach a suitable request point and maintain sufficient connectivity after submission, so that the response can be retrieved before the current primitive is exhausted.

To address this issue, we propose a communication and motion co-design framework for robot execution with foundation model inference in the cloud under unstable connectivity. The framework first estimates the time required for the next cloud request–response cycle, then uses this estimate to choose a suitable request point, guide the robot toward that point before submission, and maintain sufficient connectivity while the response is pending. Specifically, the request–response window denotes the estimated duration from request submission to response retrieval, covering network transfer and cloud inference time estimated from recent observations. Using this window, the planner selects a request point, defined as the position from which the next cloud request is submitted. The selected point is chosen to preserve progress toward the current target, avoid excessive detour, and retain a downstream opportunity for response retrieval. The request point is incorporated into a Model Predictive Path Integral (MPPI) local planner as a temporary local target before request submission. After submission, the planner resumes tracking the current primitive target while activating communication-aware costs until the next result is buffered. These costs discourage trajectories that would move into weak connectivity regions or exhaust the current primitive too early. Thus, MPPI shapes motion so that task progress, request submission, and response retrieval remain compatible during execution.

We evaluate the framework in an indoor wireless scenario built from measurements with spatially degraded connectivity. The results show that selecting where to submit cloud requests is critical for maintaining execution continuity: compared with baselines, the proposed method achieves the best or tied-best task success while using fewer request attempts and producing lower request failure and overlap rates. These results indicate that reliable cloud interaction during robot motion cannot be achieved by asynchronous timing or repeated polling alone, but requires request placement that accounts for the communication map and the remaining support of the current primitive.

The main contributions of this work are as follows:

- We formulate robot execution with cloud foundation model inference under spatially heterogeneous connectivity as a joint communication and motion problem, and introduce the request–response window to characterize whether asynchronous cloud requests can be completed before the current primitive expires.
- We develop a communication-aware execution framework that treats the next cloud request point as a motion decision during ongoing primitive execution. The framework selects a communication-favorable request point and incorporates it into an MPPI local planner, allowing the

robot to move toward the selected point while preserving task progress.

- We evaluate the framework in a measurement-based indoor wireless scenario. Compared with stop-and-wait execution, inference-only asynchrony, and fixed-period polling, the proposed method achieves higher or comparable task success with fewer request attempts and lower failure rates.

## II. RELATED WORK

Foundation models have been widely explored for semantic understanding, task planning, and action generation in open robotic environments [1]–[3], [8]–[12], [21]. For mobile robots that rely on cloud-hosted models, execution performance is also affected by the communication process that connects local motion with remote inference. We therefore review two closely related directions: latency mitigation through computation and offloading and communication-aware motion planning.

### A. Latency Mitigation through Computation and Offloading

To address the latency in cloud/edge execution pipelines, existing cloud/edge robotics studies have mainly mitigated the problem from system- and execution-level perspectives. One line of work focuses on the deployment, configuration, and reliability of remote computing services, reducing the latency of remote module invocation through computation migration, cloud resource selection, service replication, and network interface selection [17]–[20]. Another line of work directly studies Large Language Model (LLM) inference offloading, cloud-edge collaborative inference, and resource allocation. Existing studies assign LLM requests to cloud or edge servers while jointly considering bandwidth, computation resources, GPU memory, inference latency, and output quality [22], or further study edge–cloud partitioned inference for VLA models [23]. Subsequent work further summarizes communication-computation coordination problems in LLM inference, training, caching, and transmission from the perspective of mobile edge intelligence [24], or selects suitable collaborative inference paths among heterogeneous edge experts, local models, and cloud models to trade off quality, latency, energy consumption, and usage cost [25], [26]. In addition, asynchronous VLA systems attempt to maintain local reactive execution while remote semantic inference is still pending [14], [15], [27]. These studies reduce the impact of remote calls on the execution of robots or mobile terminals, but they mainly address how cloud services are deployed, invoked, scheduled, or latency-masked.

However, reducing the average latency of remote calls alone is insufficient to guarantee task continuity, because the robot’s locations at request submission and response retrieval also affect whether communication is available. Existing latency mitigation and cloud-edge collaboration methods usually treat the request submission location as a consequence of the robot’s current state, rather than as a motion decision variable that should be actively optimized. Therefore, these methods do not directly answer when and where the robot should initiate the next cloud request during ongoing execution.

## B. Communication-Aware Motion Planning

Another directly related line of research is communication-aware motion planning, which incorporates wireless communication quality into robot motion planning and control. Early work on communication-aware motion planning in mobile networks showed that robot motion affects wireless link quality, and that communication performance can therefore be optimized through trajectory design [28]. Related work also uses the directionality of signal strength to adjust robot positions and provide adaptive communication coverage in multi-robot systems [29]. Studies on motion and communication co-optimization further show that path planning, online channel estimation, and communication resources can be incorporated into a unified optimization framework [30]–[32]. For communication maps and connectivity-region modeling, some methods use wireless measurements or radio maps to discover connectable regions or recover connectivity when link quality degrades [33], [34]. These studies establish the basic premise of our work: wireless communication quality is not a uniform background condition, but a spatial field that varies with robot location.

Many communication-aware planning methods further model communication as a persistent path-level or team-level constraint, using measured or predicted signal quality, radio coverage maps, or communication-graph connectivity to maintain link availability or network connectivity [35]–[38]. Such formulations emphasize maintaining communication over an extended execution period. Other works relax the requirement of all-time connectivity by planning intermittent communication events and communication locations for multi-robot information exchange [39], [40]. Edge-assisted navigation also couples motion planning with computation and communication constraints by switching between local and edge planners during execution [41]. Beyond these works, some studies also treat the location of communication itself as a planning variable, selecting relay stops or transmission points according to link quality, data demand, or relay tasks [42]–[44]. Another related direction optimizes what information should be transmitted under communication constraints, for example by compressing task-relevant map information for online path planning [45]. Together, these works show that communication-aware planning can optimize link maintenance, transmission locations, and transmitted content, but they do not address where a robot should submit a cloud inference request whose result is needed for continued semantic execution.

These two lines of research address the challenges from different perspectives. Cloud/edge execution and inference offloading methods reduce the cost or latency of remote inference, but usually do not decide where a moving robot should submit the next request. Communication-aware motion planning methods exploit robot motion to maintain connectivity or choose transmission locations, but are not designed around delayed foundation model inference whose result is needed for continued semantic execution. In contrast, this work focuses on the coupling between local motion progress, spatially varying connectivity, and the next cloud interaction. Using a request–

response window estimated from empirical measurements, while the central decision is to select a communication-favorable request point that preserves task progress during ongoing execution.

## III. METHODOLOGY

This section presents the proposed communication-motion co-design framework, which couples high-level task scheduling with low-level robot navigation to coordinate local execution with cloud reasoning. We first describe the hierarchical the cloud–local architecture in Sec. III-A, and then formulate the system model and the validity horizon in Sec. III-B. Based on this formulation, the framework consists of three components, as summarized in Fig. 2:

- *Request–Response Window Estimation* (Sec. III-C), which estimates the stable connectivity duration required for one cloud interaction cycle by statistically predicting cloud inference latency from past observations together with network transmission time.
- *Request Point Optimization* (Sec. III-D), which computes a suitable request point such that the next cloud request can be submitted from a communication-sufficient region while still preserving a downstream opportunity to retrieve the returned result after passing that point.
- *Communication-Aware Local Path Planning* (Sec. III-E), which guides the robot toward the current active target, either the optimized request point or the task primitive target provided by cloud, while incorporating communication-aware soft constraints after the request has been submitted and until the next cloud result has been buffered locally.

### A. Cloud–Local Architecture

We address the challenge of enabling autonomous robots to execute long-horizon tasks driven by foundation models hosted in cloud, where the separation of cognitive reasoning and physical execution is essential. To support this operation, we adopt a hierarchical control architecture that enforces a strict functional partitioning between the cloud foundation model and the local controller. The cloud foundation model provides semantic guidance. It processes high-dimensional multimodal inputs to interpret user intents and generates abstract task policies rather than precise motor commands. In contrast, the local controller operates as the onboard execution unit responsible for real-time geometric grounding and safety assurance. It maps the cloud-derived semantic intent onto the robot’s physical constraints and the local environment to generate feasible trajectories.

We illustrate this division of labor through two representative scenarios. In a 2D visual navigation task, the cloud model analyzes the visual feed to identify a target object and outputs a coarse destination coordinate or a topological node representing the target semantic region. It does not account for local dynamics or ground traversability. Upon receiving this goal, the local controller employs a path planning algorithm to navigate the robot towards the target while operating within the locally available traversable space. Here, the cloud

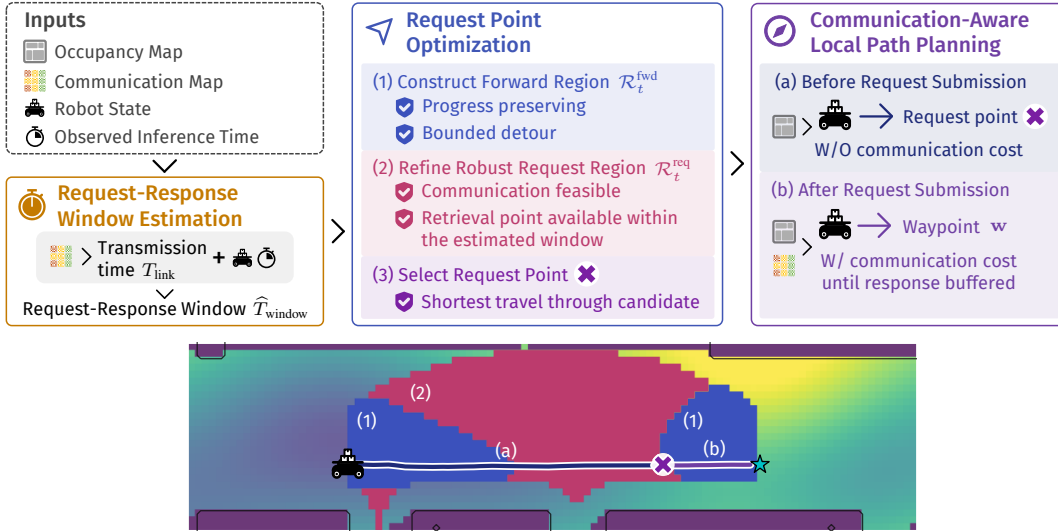


Fig. 2. System overview. Request–response window estimation estimates the request–response window required for one cloud interaction cycle from network transmission time and observed inference latency. Using this window, Request point optimization refines the forward region into the robust request region and selects a request point that supports request submission and downstream response retrieval. Communication-aware local path planning then uses the selected request point as the active target before submission, and switches to the current waypoint after submission with communication-aware soft constraints until the response is buffered.

provides the navigational intent, while the local system ensures execution under onboard geometric and safety constraints.

In a 3D mobile manipulation task, the functionality is further specialized. The cloud model identifies the target object from the scene and specifies the manipulation policy, such as the grasp type and approach direction, based on visual affordance cues. However, the cloud lacks precise knowledge of the robot’s kinematic limits and real-time joint states. Therefore, the local controller must calculate the necessary base placement to enable the manipulator to reach the 3D target defined by the cloud. Through this partitioning, the high-latency cloud loop handles the versatility of semantic understanding, while the high-frequency local loop ensures geometric feasibility and stability.

### B. Problem Formulation: System Modeling

Let  $\mathbf{x}(t)$  denote the full system state. For a navigation task,  $\mathbf{x}(t)$  reduces to the robot base pose, whereas for a mobile manipulation task it may additionally include manipulator joint states. We denote by  $\mathbf{r}(t) = [x(t), y(t)]^\top \in \mathbb{R}^2$  the planar position component of the mobile base extracted from  $\mathbf{x}(t)$ . Let  $k$  index the sequence of cloud requests, and let  $p(k)$  denote the primitive returned by the  $k$ -th request. The currently active primitive  $p(k)$  denotes the cloud-provided task instruction under execution. Although  $p(k)$  may involve the coordination of the mobile base and other actuators, its execution induces a local motion objective for the base. For local planning and execution, we represent this objective by a 2D base waypoint  $\mathbf{w} \in \mathbb{R}^2$ . Depending on the capabilities of the foundation model,  $\mathbf{w}$  may be either explicitly provided by the cloud, for example as a navigation coordinate, or implicitly derived by a local kinematic module from a higher-dimensional task goal  $\mathbf{g}_{\text{task}}$ , for example as a stance pose for object manipulation.

In this framework, we assume that the robot operates in a wireless communication environment, such as a 5 GHz Wi-Fi or 5G system, where signal quality varies across space. We further assume the availability of an environmental communication map, denoted as  $\mathcal{M}(\mathbf{r})$ , which provides an indicator of communication quality at each location, such as Received Signal Strength Indicator (RSSI) in Wi-Fi environments or Reference Signal Received Power (RSRP) in 5G systems. This map allows the robot to query the expected communication condition at any workspace location  $\mathbf{r}$  and thereby supports local estimation of the communication cost associated with a cloud interaction.

Based on this system abstraction, the next subsection quantifies the communication time required for one cloud interaction cycle.

### C. Request–Response Window Estimation

To maintain seamless autonomy, the robot should obtain the subsequent primitive  $p(k+1)$  before the current one can no longer sustain continued task progress. In our setting, this requires the next request to the cloud model to be issued sufficiently early, so that the corresponding request–response cycle can be completed without interrupting ongoing motion. We refer to the time window that must be reserved for this cycle as the request–response window. It spans the interval from request submission to response retrieval, and includes uplink transmission, cloud model inference, downlink retrieval, and an uncertainty margin for inference latency.

Among these components, cloud inference latency is particularly important because it varies with the task and can fluctuate across requests. Unlike conventional cloud computing settings, where transmission delay is often the primary concern, inference procedure by foundation models introduces an additional reasoning latency that must be predicted online.

Assuming the computational load is consistent for similar task types, we estimate the inference latency using an Exponential Weighted Moving Average (EWMA) to smooth fluctuations. The predicted inference time  $\widehat{T}_{\text{infer}}(k+1)$  and its estimated variance  $\sigma_{\text{infer}}^2(k+1)$  are updated recursively as:

$$\widehat{T}_{\text{infer}}(k+1) = \alpha T_{\text{infer}}^{\text{obs}}(k) + (1-\alpha) \widehat{T}_{\text{infer}}(k) \quad (1)$$

$$\sigma_{\text{infer}}^2(k+1) = \alpha \left( T_{\text{infer}}^{\text{obs}}(k) - \widehat{T}_{\text{infer}}(k) \right)^2 + (1-\alpha) \sigma_{\text{infer}}^2(k) \quad (2)$$

where  $k$  indexes cloud interaction cycles and  $\alpha \in (0, 1)$  is a smoothing factor,  $\widehat{T}_{\text{infer}}(0) = T_{\text{infer}}^{\text{obs}}(0)$ ,  $\sigma_{\text{infer}}^2(0) = 0$ .

The remaining components of the window are the uplink and downlink transmission times. In cloud-based inference, the uplink often carries visual observations for the foundation model, whereas the downlink returns a compact primitive. We therefore first model the uplink transmission, which is the dominant communication component in our setting. The uplink throughput  $R_{\text{up}}(\mathbf{r})$  at location  $\mathbf{r}$  is estimated by approximating an effective uplink SNR from the environmental communication map. Specifically, the effective uplink SNR is estimated from the communication-related signal level at  $\mathbf{r}$  provided by the map as

$$\text{SNR}_{\text{up}}(\mathbf{r}) = \mathcal{M}(\mathbf{r}) - \Delta P_{\text{tx}} - N_{\text{noise}}, \quad (3)$$

where  $\Delta P_{\text{tx}}$  is a calibrated uplink asymmetry term that accounts for the effective degradation of the uplink relative to the downlink, and  $N_{\text{noise}}$  denotes the noise floor. As the effective SNR decreases, the link becomes more error-prone. We characterize the Packet Error Rate (PER), denoted as  $\rho(\mathbf{r})$ , using a logistic waterfall curve that captures the sharp degradation of link reliability near the receiver sensitivity threshold  $\text{SNR}_{\text{th}}$ :

$$\rho(\mathbf{r}) = \frac{1}{1 + e^{\kappa \cdot (\text{SNR}_{\text{up}}(\mathbf{r}) - \text{SNR}_{\text{th}})}}, \quad (4)$$

where  $\kappa$  determines the steepness of the transition. The resulting expected goodput  $R_{\text{up}}(\mathbf{r})$  is modeled by accounting for rate adaptation and the retransmission overhead induced by packet errors:

$$R_{\text{up}}(\mathbf{r}) = R_{\text{link}}(\mathbf{r}) \cdot (1 - \rho(\mathbf{r}))^\gamma, \quad (5)$$

where  $R_{\text{link}}(\mathbf{r})$  denotes the baseline link rate after rate adaptation at location  $\mathbf{r}$ , and  $\gamma \geq 1$  is the congestion penalty factor. Accordingly, for an uplink payload of size  $D_{\text{up}}$ , the uplink transmission latency is

$$T_{\text{up}}(\mathbf{r}) = \frac{D_{\text{up}}}{R_{\text{up}}(\mathbf{r})}. \quad (6)$$

The downlink latency  $T_{\text{down}}(\mathbf{r})$  is computed analogously using the downlink payload size  $D_{\text{down}}$ .

Finally, to account for uncertainty in cloud inference latency, we augment the predicted inference time with a confidence margin. By scaling the standard deviation with a confidence coefficient  $\beta$ , the request–response window is estimated as

$$\widehat{T}_{\text{window}}(k+1, \mathbf{r}) = T_{\text{up}}(\mathbf{r}) + T_{\text{down}}(\mathbf{r}) + \widehat{T}_{\text{infer}}(k+1) + \beta \sigma_{\text{infer}}(k+1), \quad (7)$$

where  $\beta \sigma_{\text{infer}}(k)$  acts as a dynamic safety buffer. A more exact request–response model would distinguish the submission location from the later retrieval location of the cloud response. In our formulation, however, the request–response window is evaluated using a single-location approximation. This approximation is motivated by online tractability and by the payload asymmetry discussed above: the returned primitive is compact compared with the uploaded observation, making the uplink transmission and cloud inference time the dominant contributors to the interaction duration. Accordingly, both transmission terms are evaluated at the same candidate location when estimating  $\widehat{T}_{\text{window}}$ . This approximation is used only for local window estimation; the eventual recoverability of the cloud response after request submission is enforced separately in the request point optimization stage through a downstream feasibility condition.

#### D. Request Point Optimization

The request–response window estimated in Sec. III-C converts the asynchronous cloud interaction into a local lead-time requirement. The planner then uses this estimate together with the communication map to select where the next request should be submitted. The objective is to submit the request from a communication-favorable region while ensuring that the returned primitive can still be received as the robot continues toward the current waypoint. Accordingly, once the current waypoint  $\mathbf{w}$  becomes available, the planner computes an optimized request point  $\mathbf{p}^*$  for the subsequent cloud request. The robot first moves toward  $\mathbf{p}^*$  and issues the next request upon reaching it. It then continues toward the current waypoint  $\mathbf{w}$  while waiting for the subsequent cloud response. In this way, the execution of the current instruction and the preparation of the next interaction are explicitly coupled within a single cycle.

To compute such a request point, we first consider candidate submission locations along the remaining motion toward  $\mathbf{w}$ . We formulate this selection through a sequence of candidate filters. Let  $\mathcal{C}_{\text{free}} \subset \mathbb{R}^2$  denote the collision-free workspace for the mobile base, accounting for the robot footprint and a safety margin, and let  $\tau_{\text{move}}(\mathbf{a}, \mathbf{b})$  denote the estimated travel time from  $\mathbf{a}$  to  $\mathbf{b}$ . First, to exclude points that lie behind the robot or induce excessive detours, we define the forward region as

$$\mathcal{R}_t^{\text{fwd}} = \left\{ \mathbf{p} \in \mathcal{C}_{\text{free}} \mid \begin{aligned} &\tau_{\text{move}}(\mathbf{p}, \mathbf{w}) < \tau_{\text{move}}(\mathbf{r}(t), \mathbf{w}), \\ &\tau_{\text{move}}(\mathbf{r}(t), \mathbf{p}) + \tau_{\text{move}}(\mathbf{p}, \mathbf{w}) \leq \tau_{\text{move}}(\mathbf{r}(t), \mathbf{w}) + \varepsilon_{\text{det}} \end{aligned} \right\}, \quad (8)$$

where  $\varepsilon_{\text{det}} \geq 0$  is the allowed detour margin. The first condition requires the candidate point  $\mathbf{p}$  to be closer to the current waypoint than the robot's present position, so that it lies in the direction of ongoing task progress. The second condition bounds the additional detour incurred by visiting  $\mathbf{p}$  before resuming motion toward  $\mathbf{w}$ .

Since the forward region only enforces task progress and bounded detour, we further check whether each candidate preserves a downstream retrieval opportunity after request

submission. For any  $\mathbf{p} \in \mathcal{R}_t^{\text{fwd}}$ , we define its downstream retrieval margin as

$$\Delta_t^{\text{ret}}(\mathbf{p}) = \max_{\mathbf{q} \in \mathcal{R}_t^{\text{fwd}}} \left\{ \tau_{\text{move}}(\mathbf{p}, \mathbf{q}) - \widehat{T}_{\text{window}}(k+1, \mathbf{p}) \mid \tau_{\text{move}}(\mathbf{q}, \mathbf{w}) < \tau_{\text{move}}(\mathbf{p}, \mathbf{w}), \mathcal{M}(\mathbf{q}) \geq S_{\text{ret}} \right\}. \quad (9)$$

If no such  $\mathbf{q}$  exists, we set  $\Delta_t^{\text{ret}}(\mathbf{p}) = -\infty$ . This margin is the largest slack between the time required to move from  $\mathbf{p}$  to a downstream communication-feasible point  $\mathbf{q}$  and the estimated request–response window for obtaining  $p(k+1)$ . Thus, a positive margin indicates that at least one downstream point can serve as a feasible retrieval opportunity while the robot continues toward the current waypoint.

Based on this quantity, the robust request region is defined as

$$\mathcal{R}_t^{\text{req}} = \left\{ \mathbf{p} \in \mathcal{R}_t^{\text{fwd}} \mid \mathcal{M}(\mathbf{p}) \geq S_{\text{sub}}, \Delta_t^{\text{ret}}(\mathbf{p}) \geq \varepsilon_{\text{safe}} \right\}, \quad (10)$$

where  $S_{\text{sub}}$  and  $S_{\text{ret}}$  denote the minimum communication thresholds required for request submission and response retrieval, respectively, and  $\varepsilon_{\text{safe}} \geq 0$  is the minimum safety margin. Under the adopted window estimate, this region retains candidate submission points that satisfy the request transmission condition and still leave enough time to reach a downstream communication-feasible point for response retrieval.

Finally, the request point is selected from the robust request region by minimizing the motion cost of reaching the current waypoint through the candidate point:

$$\mathbf{p}^* = \underset{\mathbf{p} \in \mathcal{R}_t^{\text{req}}}{\text{argmin}} (\tau_{\text{move}}(\mathbf{r}(t), \mathbf{p}) + \tau_{\text{move}}(\mathbf{p}, \mathbf{w})). \quad (11)$$

This criterion selects a communication- and timing-feasible request point that introduces the smallest additional motion cost with respect to the current waypoint. Consequently, the robot is guided toward a request point only when it is compatible with the ongoing task motion, rather than being drawn to an isolated communication-favorable location. The resulting behavior preserves task progress while avoiding unnecessary detours for request submission.

If  $\mathcal{R}_t^{\text{req}} = \emptyset$ , no request point is committed at the current cycle. The robot instead continues executing toward  $\mathbf{w}$  and recomputes  $\mathcal{R}_t^{\text{req}}$  online in subsequent control cycles. Once the region becomes nonempty, its request point is adopted as the new  $\mathbf{p}^*$ . If a feasible request point still cannot be obtained after three consecutive recomputations, the planner falls back to submitting the request immediately at the next communication-favorable position encountered along the current motion.

### E. Communication-Aware Local Path Planning

The local planner generates motion while respecting robot dynamics, collision avoidance, and communication requirements. Its nominal task objective remains the current waypoint. After the request aware phase has been activated, the optimized request point is introduced as an additional short horizon reference, so that local motion is biased toward a communication favorable region without interrupting progress on the current

task. To achieve this, we formulate local motion generation as a constrained optimization and solve it using MPPI control. A sampling based formulation is particularly suitable in our setting because both the obstacle constrained feasible set and the spatial communication field may be highly irregular.

At each control time  $t$ , MPPI rolls out predicted trajectories from the current system state  $\mathbf{x}(t)$ . Let  $\ell = 0, \dots, H$  denote the prediction step index within the local horizon  $H$ . For a predicted trajectory, we write

$$\mathbf{x}_\ell = [x_\ell, y_\ell, \theta_\ell]^\top, \quad \mathbf{u}_\ell = [v_\ell, \omega_\ell]^\top, \quad (12)$$

and  $\mathbf{r}_\ell = [x_\ell, y_\ell]^\top$  denotes the predicted planar position. Let  $\xi = \{\mathbf{x}_\ell, \mathbf{u}_\ell\}_{\ell=0}^H$  denote a predicted trajectory,  $\mathbf{g}(t)$  denote the active local goal used by the planner. Before request submission,  $\mathbf{g}(t)$  may be the optimized request point  $\mathbf{p}^*(k+1)$ ; after submission, it returns to the current waypoint  $\mathbf{w}(k)$  while the robot waits for  $p(k+1)$ . Consequently, the planner optimizes a control sequence over a horizon of  $H$  steps:

$$\begin{aligned} \min_{\mathbf{u}_{0:H-1}} \quad & \lambda_n J_{\text{nav}}(\xi; \mathbf{g}(t)) + \lambda_u J_{\text{ctrl}}(\xi) + \alpha_t \cdot J_{\text{ca}}(\xi) \\ \text{s.t.} \quad & \mathbf{x}_{\ell+1} = f(\mathbf{x}_\ell, \mathbf{u}_\ell), \quad \ell = 0, \dots, H-1, \\ & \mathbf{r}_\ell \in \mathcal{C}_{\text{free}}, \quad \ell = 1, \dots, H, \\ & \mathbf{u}_\ell \in \mathcal{U}, \quad \ell = 0, \dots, H-1. \end{aligned} \quad (13)$$

Here,  $f(\cdot)$  denotes the robot kinematic model, and  $\mathcal{U}$  denotes the admissible control set with  $|v| \leq v_{\text{max}}$  and  $|\omega| \leq \omega_{\text{max}}$ . The gate  $\alpha_t \in \{0, 1\}$  controls whether the auxiliary cost  $J_{\text{ca}}$  is included in the local rollout objective. It is set to 1 only after the next cloud request has been issued and remains active until the corresponding response is buffered locally. Outside this interval,  $\alpha_t = 0$ , and the local planner reduces to the nominal navigation and control regularization objective. Thus, request point selection is handled outside the local MPPI update; the local planner only modifies the rollout cost during the interval between request submission and response buffering.

We next specify the individual cost terms that compose the local objective. First, the navigation objective promotes trajectory-level convergence toward the active goal  $\mathbf{g}_t$ . We penalize the deviation of the predicted trajectory from the active goal over the horizon:

$$J_{\text{nav}}(\xi; \mathbf{g}(t)) = \sum_{\ell=1}^H \lambda_\ell \|\mathbf{r}_\ell - \mathbf{g}(t)\|^2, \quad \lambda_\ell = \frac{\ell}{H}. \quad (14)$$

Here, the weights  $\lambda_\ell$  increase with the prediction step so that later predicted positions are penalized more strongly. The same navigation form is used whether the active goal is the optimized request point before submission or the current waypoint after submission.

Next, to improve execution smoothness, we include a small regularization term on control variation:

$$J_{\text{ctrl}}(\xi) = \frac{1}{H} \sum_{\ell=0}^{H-1} \|\mathbf{u}_\ell - \mathbf{u}_{\ell-1}\|^2, \quad (15)$$

where  $\mathbf{u}_{\ell-1}$  denotes the previously executed control. This term suppresses oscillatory commands and improves closed-loop stability.

Last, after a request has been submitted, and until the corresponding response is buffered locally, the local planner includes communication quality as a soft cost to discourage predicted rollouts from moving into weak-coverage regions. During this interval, it also penalizes rollouts that would reach the current waypoint before the returned primitive becomes available. We therefore group the communication penalty and the arrival time penalty into a single communication-aware auxiliary cost:

$$J_{ca}(\xi) = \lambda_c J_{comm}(\xi) + \lambda_a J_{arr}(\xi), \quad (16)$$

where  $\lambda_c$  and  $\lambda_a$  control the relative importance of maintaining communication quality and delaying premature arrival, respectively.

We define the communication penalty as

$$J_{comm}(\xi) = \frac{1}{H} \sum_{\ell=1}^H \left[ \max \left( 0, \frac{S_{ret} - \mathcal{M}(\mathbf{r}_\ell)}{\Delta_S} \right) \right]^2, \quad (17)$$

where  $S_{ret}$  denotes the minimum communication quality required for reliable response retrieval, and  $\Delta_S$  is a scaling factor. This term is zero in sufficiently strong coverage and increases smoothly when a predicted rollout enters weak-coverage areas.

After request submission, the robot continues moving toward the current waypoint while waiting for the returned primitive. If a rollout reaches the current waypoint before the response is buffered locally, the executable content of the current primitive is exhausted and the robot has no subsequent target to pursue. This breaks the intended pipelined execution and reduces the system to a stop-and-wait behavior at the waypoint. We therefore introduce an arrival time penalty that discourages such premature arrival. We define

$$J_{arr}(\xi) = \left[ \max(0, \widehat{T}_{window}(k+1, \mathbf{p}^*) - (t - t_{req}) - (H\Delta t + \tau_{move}(\mathbf{r}_H, \mathbf{w})) \right]^2. \quad (18)$$

Here,  $t_{req}$  denotes the time at which the request for  $P(k+1)$  is issued. This term becomes positive only when a rollout is predicted to reach  $\mathbf{w}$  earlier than the estimated request–response window time, thereby discouraging premature consumption of the current waypoint until the response is buffered locally.

Having defined the rollout cost, we now describe how (13) is solved by MPPI. The MPPI sampling update is well suited to this objective because the feasible set and the communication field can be highly nonconvex. Rollouts that violate the collision constraint  $\mathbf{r}_\ell^i \in \mathcal{C}_{free}$  or the control bound  $\mathbf{u}_\ell^i \in \mathcal{U}$  are treated as infeasible and excluded from the importance-weighted update. For each feasible rollout, the trajectory score is evaluated using the same objective as in (13):

$$S(\xi^i) = \lambda_n J_{nav}(\xi^i; \mathbf{g}(t)) + \lambda_u J_{ctrl}(\xi^i) + \alpha_t J_{ca}(\xi^i). \quad (19)$$

The corresponding MPPI weight is computed as

$$\eta_i = \frac{\exp(-S(\xi^i)/\lambda)}{\sum_j \exp(-S(\xi^j)/\lambda)}, \quad (20)$$

where  $\lambda$  is the MPPI temperature parameter. The nominal control sequence is then updated by the standard importance-weighted average of the sampled perturbations.

Overall, the local MPPI planner shapes motion under dynamics and collision constraints, while request point selection is handled by the preceding optimization stage.

#### IV. EVALUATION

This section evaluates whether the proposed connectivity-aware execution framework improves execution in a measurement-based indoor wireless scenario, without introducing excessive interruption to task execution. The main question is whether asynchronous cloud requests can be integrated with robot motion by selecting suitable request locations under spatially heterogeneous connectivity, rather than relying on stopping, periodic polling, or latency compensation alone. The remainder of this section describes the experimental setup, baseline methods, parameter settings, and evaluation metrics. We then present the quantitative results under different observation ranges and analyze the corresponding request behavior and residual failure modes.

##### A. Overview

The evaluation is conducted in a ROS-integrated Gazebo simulation environment using a TurtleBot3 Burger model. The simulated robot follows the kinematic constraints of the TurtleBot3 Burger platform, while all methods share the same global task, communication map, and cloud delay model. During execution, the robot queries the cloud-provided communication map at its current position to determine whether a request can be submitted or a response can be retrieved, and to estimate the corresponding transmission cost.

To construct a wireless environment with a realistic measurement basis, we use the SYL scenario from the SODIndoorLoc dataset as the source of the communication map [46]. SODIndoorLoc provides WiFi received signal strength fingerprints collected from multiple indoor buildings, together with dense reference points, access point information, and CAD floor plans. The SYL building contains office rooms and corridors, and includes multiple dual-band access points. In our experiments, we use the fingerprints associated with MAC208, MAC40, and MAC23 to construct a floor-level communication map that represents a common indoor coverage pattern: office areas are relatively well covered, whereas corridor segments can become weakly connected due to limited nearby access point coverage. For each selected access point, the discrete RSSI measurements at reference points are interpolated over the traversable area using Gaussian process regression. At each query position, the communication quality is defined as the strongest interpolated RSSI among the selected access points, approximating association to the locally strongest available access point. The resulting floor-level communication map is shown in Fig. 3. The task route on this map passes through traversable corridors with several low-connectivity cavities. Along the route, the robot repeatedly encounters regions where request submission becomes infeasible or the estimated transmission cost increases. The scenario therefore provides a measurement-based case for evaluating whether the next cloud request can be submitted from a communication-favorable location without substantially disrupting task progress.

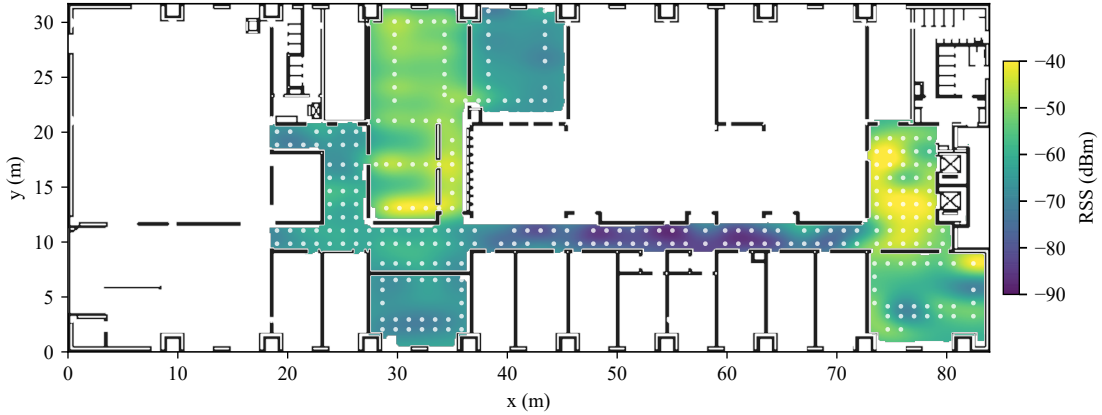


Fig. 3. Experimental environment communication map. The map is constructed from the SYL scenario of the SODIndoorLoc dataset [46] using RSS fingerprints from MAC208, MAC40, and MAC23, interpolated over the traversable area.

Cloud-generated primitives are emulated as waypoints sampled from the ROS `move_base` global path with spacing  $D_{\text{obs}}$ . To remove variability from vision-language model outputs, the cloud model is implemented as a mock VLM that returns the next waypoint on this reference path after the sampled request–response delay. All methods receive the same waypoint sequence and use the same delay model; the comparison therefore focuses on how each execution strategy handles request placement and response waiting.

All experiments are executed on the same workstation equipped with an AMD Ryzen 9950X CPU and 64 GB RAM. For all methods, the response delay is generated from the same inference and transmission model, while the robot model, global task, motion limits, and communication map are kept identical.

## B. Baselines

We compare the proposed framework with three baselines that remove different parts of communication-aware request placement. All methods use the same task route, waypoint sequence, communication map, motion limits, and cloud delay model. For the baseline methods, waypoint following and local collision avoidance are handled by `move_base`. The proposed method uses the same waypoint sequence as task guidance, but performs request-aware local execution with the MPPI planner. Therefore, the baselines evaluate different cloud request policies under a standard ROS navigation stack, while the proposed method evaluates communication-aware request placement realized through MPPI-based local execution. This comparison is consistent with recent robot execution studies that compare blocking and naive asynchronous execution to isolate the effect of inference and execution scheduling [47], and it is further motivated by recent large-model navigation systems that use fixed-rate asynchronous high-level guidance while maintaining continuous local control [48].

- **Stop-and-wait execution.** The robot requests the next primitive only after completing the currently available primitive. It then remains stopped until the next cloud response is returned. This baseline represents synchronous

cloud-guided execution without early request submission or request point repositioning.

- **Fixed-period asynchronous requests.** The robot issues cloud requests at a fixed period while continuing to follow the currently available primitive. The request timing is independent of the remaining support of the current primitive, the local communication condition, and the robot’s request location. We evaluate periods of 5, 10, and 15 s to examine how periodic request repetition affects execution continuity, request reliability, and request load.
- **Inference-only asynchronous requests.** The robot issues the next request early according to the estimated inference time  $T_{\text{infer}}$ , while continuing to execute the current primitive using `move_base`. This baseline compensates for cloud reasoning latency, but does not use the communication map to choose where the request should be issued. The request is therefore submitted along the nominal execution trajectory.

Together, these baselines distinguish the proposed request placement mechanism from three simpler alternatives: waiting for each response, polling periodically, and compensating for inference latency alone.

## C. Parameters Settings

Tab. I summarizes the main parameters used in the experiments. All baseline methods and the proposed method share the same robot model, motion limits, communication map, cloud delay model, start positions, and global goal, except for the varied observation range  $D_{\text{obs}}$ . For each value of  $D_{\text{obs}}$ , we evaluate all methods over 11 start positions,  $\{[x, 10] \mid x = 20, \dots, 30\}$ , with the same global goal  $[75, 10]$ . Changing the start position shifts where waypoint transitions occur relative to the weakly connected regions. This tests whether each method remains successful when cloud requests are needed at different locations along the same route.

## D. Metrics

We evaluate each method by measuring task completion and request behavior during robot execution. The task success

TABLE I  
EXPERIMENTAL PARAMETERS.

Symbol	Parameter	Value
$\mathbf{x}(0)$	Initial robot positions	[20, 10]–[30, 10]
$\mathbf{g}$	Global goal	[75.0, 10.0]
$v_{\max}$	Maximum linear velocity	0.22 m/s
$\Delta t$	Control interval	0.1 s
$H$	MPPI prediction horizon	30
$K$	Number of MPPI rollouts	300
$\lambda$	MPPI temperature	1.0
$\lambda_n$	Navigation cost weight	1.0
$\lambda_u$	Control regularization weight	0.005
$\lambda_c$	Communication cost weight	15.0
$\lambda_a$	Arrival time cost weight	10.0
$S_{\text{sub}}$	Uplink submission threshold	−84 dBm
$S_{\text{ret}}$	Downlink retrieval threshold	−90 dBm
$\Delta_S$	Communication cost scale	10.0 dB
$D_{\text{up}}$	Uplink payload size	5.0 MB
$D_{\text{down}}$	Downlink payload size	0.01 MB
$D_{\text{obs}}$	Waypoint spacing	{5.0, 5.5, 6.0} m
$T_{\text{infer}}$	Inference duration generation	$\mathcal{N}(6.0, 0.5^2)$ s
$\Delta P_x$	Uplink asymmetry offset	6.0 dB
$\alpha$	EWMA smoothing factor	0.3
$\beta$	Inference uncertainty coefficient	1.0
$\hat{T}_{\text{infer}}(0)$	Initial inference time estimate	6.0
$\varepsilon_{\text{det}}$	Detour margin	4 s
$\varepsilon_{\text{safe}}$	Retrieval safety margin	0.5 s

rate  $R_{\text{succ}}$  is reported as the percentage of start cases in which the robot reaches the prescribed global goal  $\mathbf{g}$ . The request–response window  $T_{\text{window}}$  is reported to characterize the duration of the cloud cycle associated with issued requests. The number of cloud requests  $N_{\text{req}}$  counts the request attempts generated during execution and serves as a proxy for request load. The waiting time  $T_{\text{wait}}$  measures the time for which the robot is blocked because the next cloud result is not yet available. Unlike accumulated execution time, this quantity isolates the blocking time induced by the request–response process. The request failure rate  $R_{\text{fail}}$  is computed as the fraction of failed requests among all issued requests, reflecting whether requests are issued from communication-favorable states. The overlap rate  $R_{\text{ovl}}$  is defined as the fraction of requests initiated while a previous request–response cycle is still unresolved. It indicates whether a method keeps multiple cloud requests outstanding to maintain task progress. All quantities except  $R_{\text{succ}}$  are reported as mean  $\pm$  standard deviation over start cases for each combination of method and observation range.

## E. Results

1) *Overall Performance*: Tab. II summarizes the overall performance under the three observation ranges. The reported request–response window remains on the same time scale across methods, with mean values between 6.4 and 6.9 s. Since all methods use the same inference duration model and communication map, the performance differences are interpreted through how each execution policy places, repeats, or waits for cloud requests under spatially heterogeneous connectivity. The stop-and-wait baseline exposes two coupled limitations of synchronous execution: the robot is blocked by cloud latency after each primitive, and the next request must be uploaded from the location reached after the previous waypoint. If this

location lies in a weakly connected region, the next request itself becomes unreliable. Inference-only async reduces latency-induced blocking by triggering requests earlier, but it does not use the communication map to actively choose where the request should be issued. The request location therefore remains determined by the natural execution trajectory, and the method can suffer from the same location-dependent upload failures as stop-and-wait execution. Fixed-period async acts as a redundancy-based baseline: shorter polling periods increase the chance that at least one request is issued from a favorable communication state, but this is obtained by issuing task-agnostic requests at a prescribed rate. As the period becomes shorter, this strategy moves toward a high-request regime and produces more overlapped cloud requests. In contrast, the proposed method achieves the highest or tied-highest task success across all observation ranges. The low waiting time, request failure rate, and overlap rate indicate that task progress is rarely blocked by unavailable responses, failed submissions, or outstanding redundant requests.

Fig. 4 provides a representative view of the proposed execution behavior. Methods without active request selection follow the nominal task route and may submit the next request after entering a weakly connected region. The proposed method instead computes downstream request points on the communication map and redirects the robot toward them before submission. In this example, the trajectory bends toward communication-favorable regions, and the actual request submissions occur near the computed request points.

Figs. 5 and 6 further show how task success is obtained. The proposed method remains in the high-success, low-request region across all tested observation ranges. At  $D_{\text{obs}} = 5.0$  m, it achieves the highest task success rate with far fewer requests than the fixed-period baselines; at  $D_{\text{obs}} = 5.5$  m and 6.0 m, it matches the best fixed-period baselines while using substantially fewer requests. In contrast, fixed-period polling reaches high task success by increasing request attempts. For example, at  $D_{\text{obs}} = 6.0$  m, fixed-period 5s achieves 100.0% task success but requires  $50.5 \pm 3.4$  requests and produces an overlap rate of  $51.5 \pm 0.7\%$ , whereas the proposed method achieves the same task success with  $15.3 \pm 1.6$  requests and no failed or overlapped requests. These results indicate that the proposed method does not improve task completion by simply increasing the number of cloud requests. Instead, it selects request locations using the robot state, the communication map, and the finite support of the current primitive, so that the next request–response cycle can be initiated from a communication-favorable position during ongoing execution. This supports the role of connectivity-aware request placement, rather than repeated polling, in producing cloud requests that are reliable, non-overlapped, and compatible with ongoing execution.

2) *Execution Time Overhead*: Fig. 7 compares the completion time of successful runs from each start position. Since only task-successful cases are plotted, the figure is used to examine whether the lower waiting time and fewer failed or overlapped requests are accompanied by a substantial execution-time penalty. The results are shown per start position because different starts have different path lengths and encounter weakly connected regions at different execution

TABLE II  
OVERALL PERFORMANCE UNDER DIFFERENT OBSERVATION RANGES.

$D_{\text{obs}}$	Method	$R_{\text{succ}} \uparrow$	$T_{\text{window}} \text{ (s)}$	$N_{\text{req}} \downarrow$	$T_{\text{wait}} \text{ (s)} \downarrow$	$R_{\text{fail}} \downarrow$	$R_{\text{owl}} \downarrow$
5.0 m	Stop-wait	18.2%	$6.7 \pm 0.4$	$25.4 \pm 7.4$	$19.4 \pm 0.3$	$62.1 \pm 30.9\%$	$0.0 \pm 0.0\%$
	Inference-only	0.0%	$6.6 \pm 0.3$	$36.8 \pm 0.6$	$8.8 \pm 0.4$	$72.8 \pm 3.5\%$	$0.0 \pm 0.0\%$
	Fixed-period 15s	27.3%	$6.7 \pm 0.4$	$28.3 \pm 6.4$	$14.0 \pm 0.3$	$51.5 \pm 25.1\%$	$0.0 \pm 0.0\%$
	Fixed-period 10s	63.6%	$6.6 \pm 0.1$	$34.8 \pm 10.6$	$10.0 \pm 0.3$	$34.5 \pm 25.6\%$	$17.3 \pm 12.4\%$
	Fixed-period 5s	72.7%	$6.6 \pm 0.2$	$63.7 \pm 20.9$	$9.9 \pm 0.2$	$63.2 \pm 12.6\%$	$54.0 \pm 4.2\%$
	Proposed	<b>81.8%</b>	$6.7 \pm 0.1$	<b><math>17.4 \pm 2.7</math></b>	<b><math>3.0 \pm 6.5</math></b>	<b><math>1.4 \pm 3.1\%</math></b>	<b><math>0.0 \pm 0.0\%</math></b>
5.5 m	Stop-wait	27.3%	$6.6 \pm 0.5$	$23.5 \pm 8.8$	$21.3 \pm 0.6$	$57.0 \pm 36.8\%$	$0.0 \pm 0.0\%$
	Inference-only	0.0%	$6.7 \pm 0.4$	$35.6 \pm 0.7$	$10.5 \pm 0.4$	$75.5 \pm 3.2\%$	$0.0 \pm 0.0\%$
	Fixed-period 15s	63.6%	$6.8 \pm 0.3$	$22.9 \pm 7.2$	$14.1 \pm 0.3$	$31.0 \pm 26.7\%$	$0.0 \pm 0.0\%$
	Fixed-period 10s	<b>100.0%</b>	$6.5 \pm 0.2$	$26.5 \pm 1.8$	$10.1 \pm 0.2$	$16.5 \pm 2.7\%$	$7.9 \pm 1.2\%$
	Fixed-period 5s	90.9%	$6.5 \pm 0.2$	$54.9 \pm 14.1$	$10.1 \pm 0.2$	$58.8 \pm 8.2\%$	$52.2 \pm 2.8\%$
	Proposed	<b>100.0%</b>	$6.8 \pm 0.1$	<b><math>16.5 \pm 1.2</math></b>	<b><math>0.1 \pm 0.1</math></b>	<b><math>0.0 \pm 0.0\%</math></b>	<b><math>0.0 \pm 0.0\%</math></b>
6.0 m	Stop-wait	36.4%	$6.7 \pm 0.2$	$21.2 \pm 10.1$	$23.2 \pm 0.6$	$50.7 \pm 40.3\%$	$0.0 \pm 0.0\%$
	Inference-only	27.3%	$6.6 \pm 0.3$	$28.9 \pm 10.3$	$12.6 \pm 0.9$	$60.2 \pm 30.7\%$	$0.0 \pm 0.0\%$
	Fixed-period 15s	81.8%	$6.7 \pm 0.2$	$20.2 \pm 5.9$	$14.5 \pm 0.3$	$22.6 \pm 22.3\%$	$0.0 \pm 0.0\%$
	Fixed-period 10s	<b>100.0%</b>	$6.4 \pm 0.1$	$26.0 \pm 1.8$	$10.3 \pm 0.2$	$16.7 \pm 2.9\%$	$8.0 \pm 0.9\%$
	Fixed-period 5s	<b>100.0%</b>	$6.6 \pm 0.2$	$50.5 \pm 3.4$	$10.3 \pm 0.3$	$56.9 \pm 1.8\%$	$51.5 \pm 0.7\%$
	Proposed	<b>100.0%</b>	$6.9 \pm 0.3$	<b><math>15.3 \pm 1.6</math></b>	<b><math>0.1 \pm 0.0</math></b>	<b><math>0.0 \pm 0.0\%</math></b>	<b><math>0.0 \pm 0.0\%</math></b>

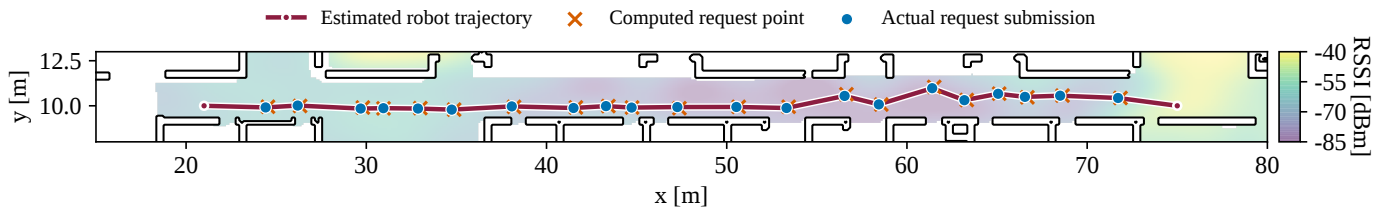


Fig. 4. Representative execution trace of the proposed method on the communication map. The proposed method actively relocates request submission toward communication-favorable regions.

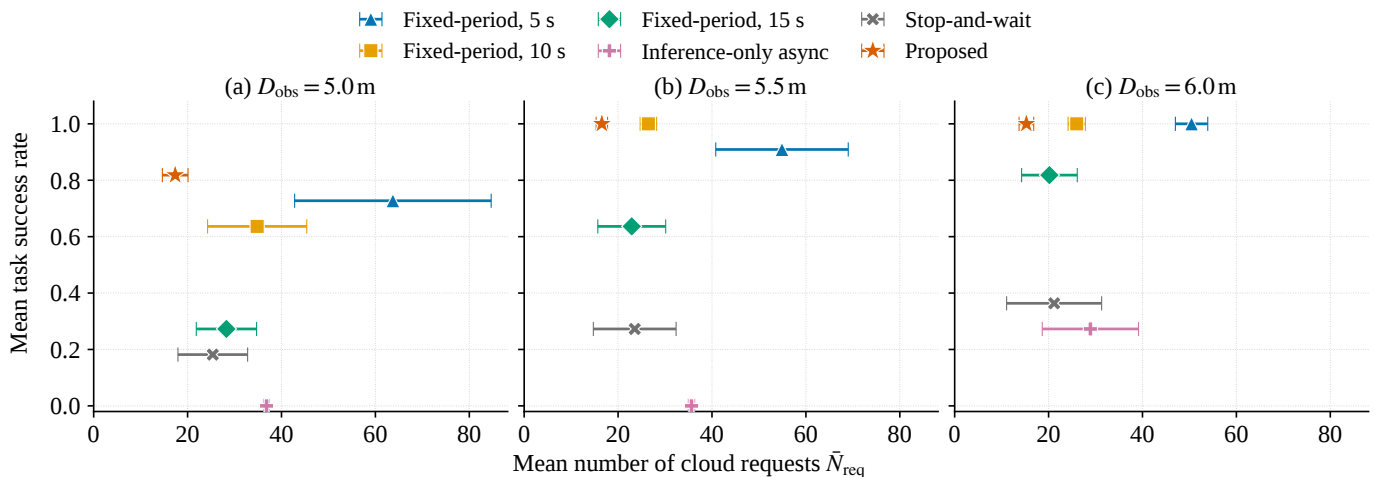


Fig. 5. Task success rate versus the mean number of cloud requests under different observation ranges. The proposed method lies in the high-success, low-request region, while short-period polling reaches high success with many more requests.

stages. Across the tested observation ranges, the proposed method remains comparable to the asynchronous baselines in successful task completion time, although it is not always the fastest method at every start position. Together with Tab. II, this suggests that the reduced waiting, failed submissions, and overlapped requests are not mainly obtained by slowing down

the robot or taking large detours.

3) *Boundary Behavior*: Fig. 8 plots the RSSI measured at request submission events for the proposed method. Most submissions remain above the feasibility threshold across the tested observation ranges, which is consistent with the low request failure rate in Tab. II. The residual failed cases at  $D_{\text{obs}} = 5.0 \text{ m}$  appear near the threshold, indicating that

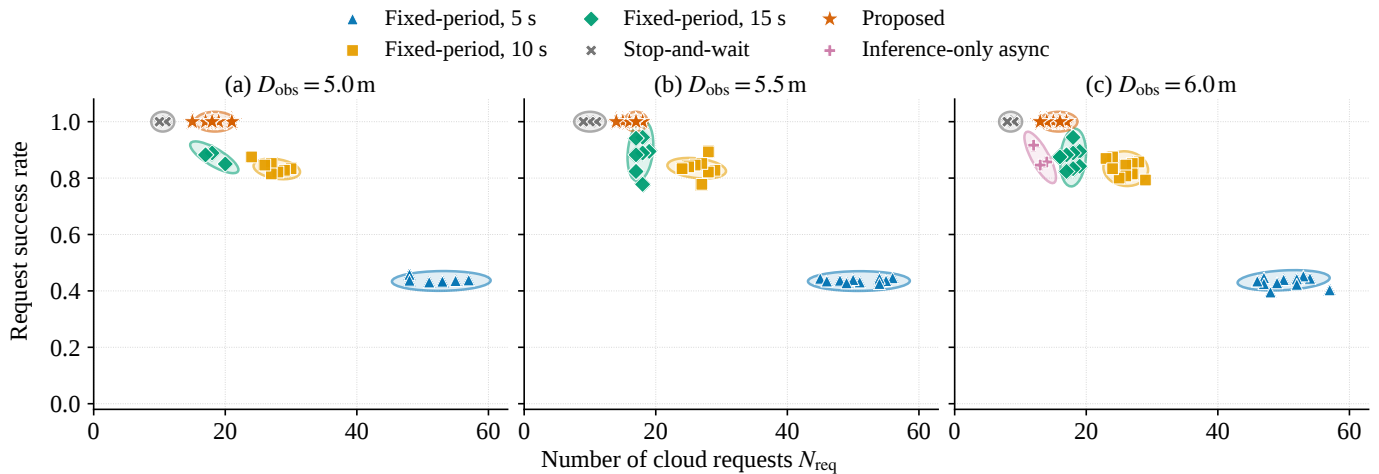


Fig. 6. Request success rate versus the number of cloud requests under different observation ranges. The plot contrasts reliable request placement with repeated request attempts.

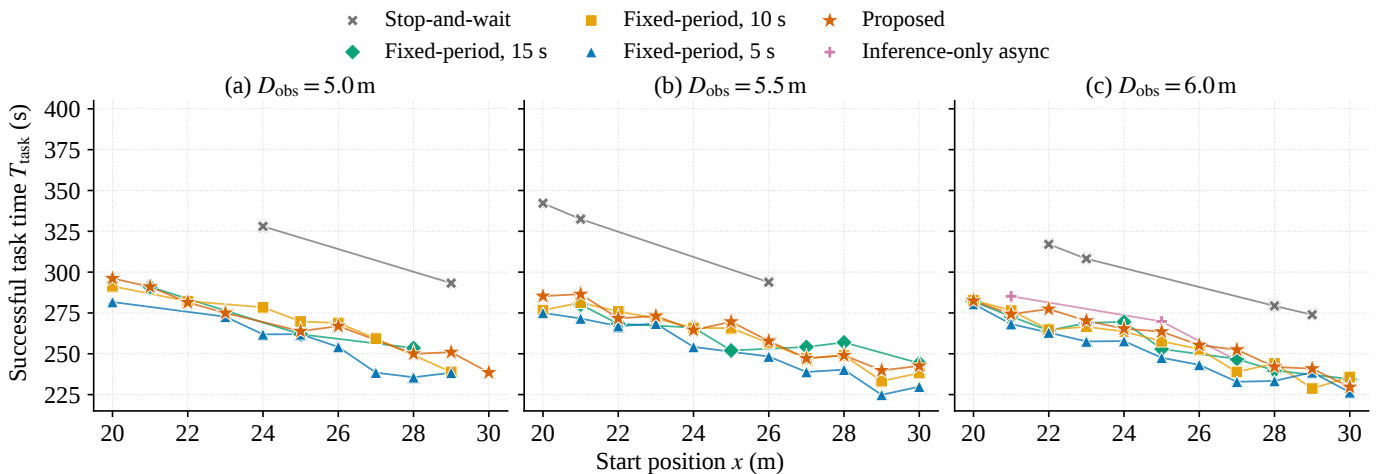


Fig. 7. Successful task completion time over different start positions. Only task-successful cases are plotted.

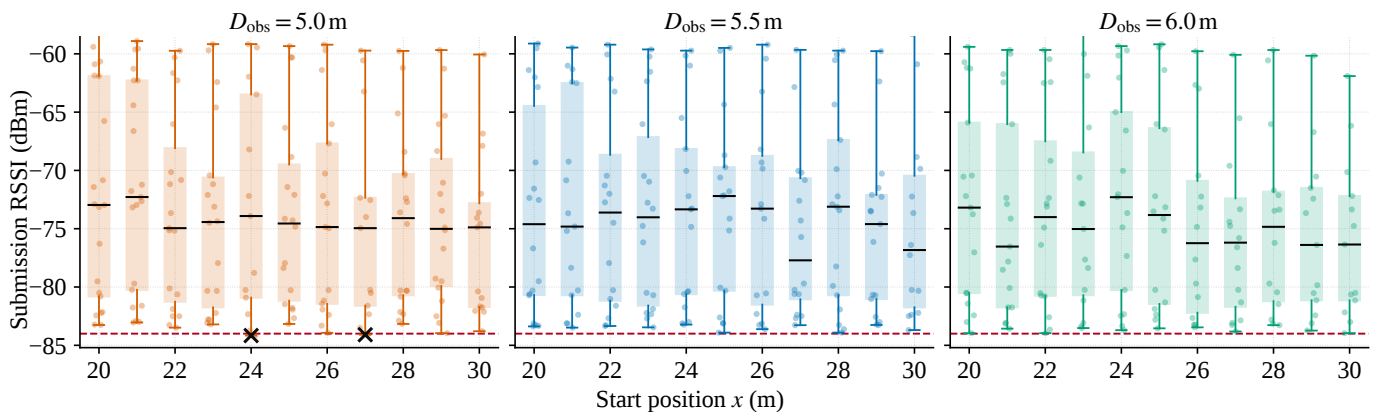


Fig. 8. RSSI measured at request submission events for the proposed method. The red dashed line denotes the feasibility threshold, and black crosses indicate residual failed cases. Most submissions remain above the threshold, while the residual failures at  $D_{\text{obs}} = 5.0$  m occur near the threshold.

they occur in a low-margin regime of point-based request placement. This behavior follows from the reduced support provided by the shorter observation range. When  $D_{\text{obs}}$  is small,

the downstream region in which a request point can simultaneously satisfy the timing constraint, the communication constraint, and the task-progress constraint becomes narrower.

The selected request point can therefore lie close to the boundary of the connected region. Since request submission is triggered when the robot reaches the request point within a finite distance tolerance, the actual submission pose may slightly differ from the nominal request point. If this difference occurs in an area with a steep local RSSI gradient, a point that is feasible on the communication map can become marginal or infeasible at execution time.

This boundary behavior also illustrates the robustness–feasibility trade-off in request point selection. Using a more conservative RSSI margin would move selected points farther inside connected regions and reduce sensitivity to small execution errors, but it would also shrink the feasible request-point set. This effect becomes more restrictive when the current primitive provides only limited forward support. A region-based representation of request opportunities could further reduce sensitivity to pose-level deviations, but it would increase online computation and weaken the immediacy required for request placement during execution. Thus, the remaining failures at  $D_{\text{obs}} = 5.0\text{m}$  mark the boundary of point-based request placement when temporal support and connectivity margin are both limited.

Taken together, the results support the proposed mechanism of relocating asynchronous request submission rather than increasing request frequency. First, the task/request tradeoff shows that the proposed method achieves the highest or tied-highest task success with fewer request attempts than the fixed-period baselines, indicating that the improvement is not obtained through repeated polling. Second, the low request failure and overlap rates show that the selected submission locations produce reliable and non-redundant request behavior. Third, the submission RSSI analysis shows that most executed requests are submitted from communication-feasible states, while the residual failures at the shortest observation range occur near the connectivity boundary. Together with the completion time results, these observations indicate that communication-aware request placement maintains task continuity by reducing request-induced waiting, failed requests, and redundant request attempts, without substantially slowing the completed executions.

## V. CONCLUSION

This paper studied robot execution based on cloud-hosted foundation model inference under spatially heterogeneous wireless connectivity. In such systems, the robot needs to continue executing the currently available cloud primitive while submitting the next cloud request at an appropriate time. Therefore, task continuity is jointly affected by motion feasibility and communication conditions. To capture this coupling, this paper introduced the request–response window to characterize the relationship between the time required for cloud interaction and the support of the current primitive. Based on this formulation, we proposed a communication-aware execution framework. The framework uses a communication map to select a suitable request point and incorporates it into local planning, thereby improving the success rate of subsequent requests and the continuity of execution while maintaining

task progress. Experiments in a measurement-based indoor wireless scenario showed that the proposed method improves the robustness of execution under spatially heterogeneous connectivity. Compared with the baseline methods, our method achieved more stable task success while reducing unnecessary request attempts and request failures. These results indicate that, in unstable or spatially varying wireless environments, robot execution relying on cloud-hosted inference cannot simply treat communication as an external service. Instead, local motion and communication opportunities need to be actively coordinated during execution.

Several directions remain for future work. First, the proposed method assumes that the communication map is available before execution, whereas in practical deployments, communication quality may be affected by human movement, occlusion, network load, and environmental changes. Therefore, reliable communication-aware execution with incomplete or dynamically changing communication maps is an important direction for future extension. Second, closed-loop experiments with online cloud inference over deployed Wi-Fi or 5G networks would help further evaluate the effectiveness and limitations of the proposed framework in practical systems. Finally, when the environment lacks communication regions that satisfy the request condition for an extended period, how the robot can maintain basic task progress through degraded execution, local fallback strategies, or task replanning is also worth further investigation.

## APPENDIX

### A. Capability Boundary of Proposed Method

Let  $\mathbf{p}_k$  denote the observation/submission location associated with request  $k$ , let  $\mathbf{w}(k)$  denote the waypoint induced by the currently active primitive  $p(k)$ , and let  $\mathbf{p}_{k+1}$  denote the request point selected for obtaining  $p(k+1)$ .

Let  $D_{\text{obs}}$  denote the maximum forward perception range of a single visual observation. The waypoint induced by the  $k$ -th observation is constrained to lie within this forward support bound. Therefore,

$$\tau_{\text{move}}(\mathbf{p}_k, \mathbf{w}(k)) \leq \frac{D_{\text{obs}}}{v_{\text{max}}}. \quad (21)$$

Here,  $D_{\text{obs}}/v_{\text{max}}$  represents the maximum motion time support induced by one observation.

After the primitive  $p(k)$  becomes active, the robot continues from  $\mathbf{p}_k$  toward  $\mathbf{w}(k)$  and issues the next request at the selected forward request point  $\mathbf{p}_{k+1}$ . For later reference, we restate the detour part of the forward admissibility condition evaluated at  $\mathbf{p}_{k+1}$ :

$$\tau_{\text{move}}(\mathbf{p}_k, \mathbf{p}_{k+1}) + \tau_{\text{move}}(\mathbf{p}_{k+1}, \mathbf{w}(k)) \leq \tau_{\text{move}}(\mathbf{p}_k, \mathbf{w}(k)) + \varepsilon_{\text{det}}. \quad (22)$$

The downstream feasibility condition used in request point optimization further requires that, after submitting the request, the robot retains enough remaining motion time to receive the returned primitive at a later communication feasible point. If we omit the explicit retrieval point and only express the

required remaining travel time after request submission, this gives

$$\tau_{\text{move}}(\mathbf{p}_{k+1}, \mathbf{w}(k)) \geq \widehat{T}_{\text{window}}(k+1, \mathbf{p}_{k+1}) + \varepsilon_{\text{safe}}. \quad (23)$$

Substituting eq. (23) into eq. (22) yields

$$\tau_{\text{move}}(\mathbf{p}_k, \mathbf{p}_{k+1}) \leq \tau_{\text{move}}(\mathbf{p}_k, \mathbf{w}(k)) - \widehat{T}_{\text{window}}(k+1, \mathbf{p}_{k+1}) - \varepsilon. \quad (24)$$

where  $\varepsilon = \varepsilon_{\text{safe}} - \varepsilon_{\text{det}}$ . Combining eq. (21) and eq. (24), we obtain

$$\tau_{\text{move}}(\mathbf{p}_k, \mathbf{p}_{k+1}) \leq \frac{D_{\text{obs}}}{v_{\text{max}}} - \widehat{T}_{\text{window}}(k+1, \mathbf{p}_{k+1}) - \varepsilon. \quad (25)$$

Eq. (25) provides a timing boundary for the proposed execution scheme. It characterizes a tradeoff between local execution autonomy and remote reasoning latency: larger communication or inference delays require the next request to be issued earlier, whereas longer motion support from the current primitive provides more opportunity for proactive request scheduling. Equivalently, the timing boundary can be expressed in distance form by representing the motion support of the current primitive as a distance budget  $D_{\text{obs}}$ . Defining the maximum request deferral length as

$$L_{\text{def},k} := v_{\text{max}} \cdot \tau_{\text{move}}(\mathbf{p}_k, \mathbf{p}_{k+1}), \quad (26)$$

we obtain

$$L_{\text{def},k} \leq D_{\text{obs}} - v_{\text{max}} \left( \widehat{T}_{\text{window}}(k+1, \mathbf{p}_{k+1}) + \varepsilon \right). \quad (27)$$

Eq. (27) can be read as an upper envelope on how far the next request may be postponed while the robot is still executing the current primitive. Since  $\widehat{T}_{\text{window}}$  contains both communication latency and cloud inference latency, the bound separates the forward motion support provided by the current observation from the time that must be reserved for the next cloud cycle. In the most favorable communication case, where uplink and downlink transmission times are negligible, this bound reduces to

$$L_{\text{def},k} \lesssim D_{\text{obs}} - v_{\text{max}} \left( \widehat{T}_{\text{infer}}(k+1) + \beta \sigma_{\text{infer}}(k+1) + \varepsilon \right). \quad (28)$$

Thus, even under ideal connectivity, the admissible travel before issuing the next request is bounded by the cloud reasoning latency and the effective timing reserve. In regions with weak connectivity, the transmission components in  $\widehat{T}_{\text{window}}$  further tighten this bound. Therefore, (27) should be interpreted as a performance upper bound of the proposed strategy: the method can maintain continuous progress only when the travel required before the next feasible request remains within the finite forward support provided by the current primitive. If a region without usable connectivity exceeds this support, request point optimization alone cannot guarantee continuity; it can only select the latest feasible downstream submission point within the available motion budget.

## REFERENCES

- [1] B. Zitkovich, T. Yu, S. Xu, P. Xu, T. Xiao, F. Xia, J. Wu, P. Wohlhart, S. Welker, A. Wahid, Q. Vuong, V. Vanhoucke, H. Tran, R. Soricut, A. Singh, J. Singh, P. Sermanet, P. R. Sanketi, G. Salazar, M. S. Ryo, K. Reymann, K. Rao, K. Pertsch, I. Mordatch, H. Michalewski, Y. Lu, S. Levine, L. Lee, T.-W. E. Lee, I. Leal, Y. Kuang, D. Kalashnikov, R. Julian, N. J. Joshi, A. Irpan, B. Ichter, J. Hsu, A. Herzog, K. Hausman, K. Gopalakrishnan, C. Fu, P. Florence, C. Finn, K. A. Dubey, D. Driess, T. Ding, K. M. Choromanski, X. Chen, Y. Chebotar, J. Carbajal, N. Brown, A. Brohan, M. G. Arenas, and K. Han, "RT-2: Vision-Language-Action Models Transfer Web Knowledge to Robotic Control," in *Proceedings of The 7th Annual Conference on Robot Learning (CoRL)*, vol. 229, 2023, pp. 2165–2183.
- [2] M. Kim, K. Pertsch, S. Karamcheti, T. Xiao, A. Balakrishna, S. Nair, R. Raffailov, E. Foster, G. Lam, P. Sanketi, Q. Vuong, T. Kollar, B. Burchfiel, R. Tedrake, D. Sadigh, S. Levine, P. Liang, and C. Finn, "OpenVLA: An Open-Source Vision-Language-Action Model," *arXiv preprint arXiv:2406.09246*, 2024.
- [3] K. Black, N. Brown, D. Driess, A. Esmail, M. Equi, C. Finn, N. Fusai, L. Groom, K. Hausman, B. Ichter, S. Jakubczak, T. Jones, L. Ke, S. Levine, A. Li-Bell, M. Mothukuri, S. Nair, K. Pertsch, L. X. Shi, J. Tanner, Q. Vuong, A. Walling, H. Wang, and U. Zhilinsky, " $\pi_0$ : A Vision-Language-Action Flow Model for General Robot Control," *arXiv preprint arXiv:2410.24164*, 2024.
- [4] H. Pan, S. Huang, J. Yang, J. Mi, K. Li, X. You, P. Liang, J. Yang, Y. Liu, J. Zhang, M. Wang, J. Yang, X. Zhang, L. Zhao, M. Chen, J. Zhou, and X. Wei, "Robot Navigation via Foundation Language Models: A Review," *ACM Comput. Surv.*, vol. 58, no. 11, 2026.
- [5] R. Firoozi, J. Tucker, S. Tian, A. Majumdar, J. Sun, W. Liu, Y. Zhu, S. Song, A. Kapoor, K. Hausman, B. Ichter, D. Driess, J. Wu, C. Lu, and M. Schwager, "Foundation models in robotics: Applications, challenges, and the future," *The International Journal of Robotics Research*, vol. 44, no. 5, pp. 701–739, 2025.
- [6] Y. Zheng, Y. Chen, B. Qian, X. Shi, Y. Shu, and J. Chen, "A Review on Edge Large Language Models: Design, Execution, and Applications," *ACM Comput. Surv.*, vol. 57, no. 8, Mar. 2025.
- [7] D. Shah, B. Osinski, B. Ichter, and S. Levine, "LM-Nav: Robotic Navigation with Large Pre-Trained Models of Language, Vision, and Action," in *Proceedings of The 6th Annual Conference on Robot Learning (CoRL)*, 2022.
- [8] J. Liang, W. Huang, F. Xia, P. Xu, K. Hausman, B. Ichter, P. Florence, and A. Zeng, "Code as Policies: Language Model Programs for Embodied Control," in *Proceedings of 2023 IEEE International Conference on Robotics and Automation (ICRA)*, 2023, pp. 9493–9500.
- [9] C. Huang, O. Mees, A. Zeng, and W. Burgard, "Visual Language Maps for Robot Navigation," in *Proceedings of 2023 IEEE International Conference on Robotics and Automation (ICRA)*, 2023, pp. 10608–10615.
- [10] K. Obata, T. Aoki, T. Horii, T. Taniguchi, and T. Nagai, "LiP-LLM: Integrating Linear Programming and Dependency Graph With Large Language Models for Multi-Robot Task Planning," *IEEE Robotics and Automation Letters*, vol. 10, no. 2, pp. 1122–1129, 2025.
- [11] J. Wang, T. Wang, W. Cai, L. Xu, and C. Sun, "Boosting Efficient Reinforcement Learning for Vision-and-Language Navigation With Open-Sourced LLM," *IEEE Robotics and Automation Letters*, vol. 10, no. 1, pp. 612–619, 2025.
- [12] F. Liu, H. Su, H. Chi, R. Geng, C. Ren, X. Liu, Y. Xu, Y. Ohsita, and L. Zhang, "Event-Driven Proactive Assistive Manipulation with Grounded Vision-Language Planning," *arXiv preprint arXiv:2603.23950*, 2026.
- [13] J. Tang, Y. Sun, Y. Zhao, S. Yang, Y. Lin, Z. Zhang, J. Hou, Y. Lu, Z. Liu, and S. Han, "VLASH: Real-Time VLAs via Future-State-Aware Asynchronous Inference," *arXiv preprint arXiv:2512.01031*, 2025.
- [14] N. Hirose, C. Glossop, D. Shah, and S. Levine, "AsyncVLA: An Asynchronous VLA for Fast and Robust Navigation on the Edge," *arXiv preprint arXiv:2602.13476*, 2026.
- [15] C. Nguyen, S. Jin, F. T. Pokorny, and E. Elmroth, "Speculative Policy Orchestration: A Latency-Resilient Framework for Cloud-Robotic Manipulation," *arXiv preprint arXiv:2603.19418*, 2026.
- [16] E. Zeydan, S. S. Arslan, Y. Turk, T. Hewa, and M. Liyanage, "The Role of Mobile Communications for Industrial Automation: Architecture, Applications and Challenges," *IEEE Open Journal of the Communications Society*, vol. 6, pp. 6808–6841, 2025.
- [17] J. Ichnowski, K. Chen, K. Dharmarajan, S. Adebola, M. Danielczuk, V. Mayoral-Vilches, N. Jha, H. Zhan, E. Llontop, D. Xu, C. Buscaron, J. Kubiatowicz, I. Stoica, J. Gonzalez, and K. Goldberg, "FogROS2:

- An Adaptive Platform for Cloud and Fog Robotics Using ROS 2,” in *Proceedings of 2023 IEEE International Conference on Robotics and Automation (ICRA)*, 2023, pp. 5493–5500.
- [18] K. Chen, M. Wang, M. Gualtieri, N. Tian, C. Juette, L. Ren, J. Ichnowski, J. Kubiawicz, and K. Goldberg, “FogROS2-LS: A Location-Independent Fog Robotics Framework for Latency Sensitive ROS2 Applications,” in *Proceedings of 2024 IEEE International Conference on Robotics and Automation (ICRA)*, 2024, pp. 10 581–10 587.
- [19] K. Chen, K. Hari, T. Chung, M. Wang, N. Tian, C. Juette, J. Ichnowski, L. Ren, J. Kubiawicz, I. Stoica, and K. Goldberg, “FogROS2-FT: Fault Tolerant Cloud Robotics,” in *Proceedings of 2024 IEEE/RSJ International Conference on Intelligent Robots and Systems (IROS)*, 2024, pp. 1390–1397.
- [20] K. Chen, N. Tian, C. Juette, T. Qiu, L. Ren, J. Kubiawicz, and K. Goldberg, “FogROS2-PLR: Probabilistic Latency-Reliability for Cloud Robotics,” in *Proceedings of 2025 IEEE International Conference on Robotics and Automation (ICRA)*, 2025, pp. 16 290–16 297.
- [21] M. T. Tariq, Y. Hussain, and C. Wang, “Robust mobile robot path planning via llm-based dynamic waypoint generation,” *Expert Systems with Applications*, vol. 282, p. 127600, 2025.
- [22] Y. He, J. Fang, F. R. Yu, and V. C. Leung, “Large Language Models (LLMs) Inference Offloading and Resource Allocation in Cloud-Edge Computing: An Active Inference Approach,” *IEEE Transactions on Mobile Computing*, vol. 23, no. 12, pp. 11 253–11 264, 2024.
- [23] Z. Zheng, S. Tian, H. Cao, C. Li, J. Chen, M. Li, X. Sun, H. Zou, G. Luo, and X. Chen, “RAPID: Redundancy-Aware and Compatibility-Optimal Edge-Cloud Partitioned Inference for Diverse VLA Models,” *arXiv preprint arXiv:2603.07949*, 2026.
- [24] G. Qu, Q. Chen, W. Wei, Z. Lin, X. Chen, and K. Huang, “Mobile Edge Intelligence for Large Language Models: A Contemporary Survey,” *IEEE Communications Surveys & Tutorials*, vol. 27, no. 6, pp. 3820–3860, 2025.
- [25] L. Yuan, D.-J. Han, S. Wang, and C. Brinton, “Local-Cloud Inference Offloading for LLMs in Multi-Modal, Multi-Task, Multi-Dialogue Settings,” in *Proceedings of the Twenty-Sixth International Symposium on Theory, Algorithmic Foundations, and Protocol Design for Mobile Networks and Mobile Computing*, 2025, p. 201–210.
- [26] L. Jin, Y. Zhang, Y. Li, S. Wang, H. H. Yang, J. Wu, and M. Zhang, “MoE2: Optimizing Collaborative Inference for Edge Large Language Models,” *IEEE Transactions on Networking*, vol. 34, pp. 4637–4651, 2026.
- [27] K. Yang, Z. Chu, Y. Guo, Z. Wang, S. Xie, Y. Shen, X. Wu, X. Li, and M. Xu, “AsyncShield: A Plug-and-Play Edge Adapter for Asynchronous Cloud-based VLA Navigation,” *arXiv preprint arXiv:2604.24086*, 2026.
- [28] A. Ghaffarkhah and Y. Mostofi, “Communication-Aware Motion Planning in Mobile Networks,” *IEEE Transactions on Automatic Control*, vol. 56, no. 10, pp. 2478–2485, 2011.
- [29] S. Gil, S. Kumar, D. Katabi, and D. Rus, “Adaptive communication in multi-robot systems using directionality of signal strength,” *The International Journal of Robotics Research*, vol. 34, no. 7, pp. 946–968, 2015.
- [30] Y. Yan and Y. Mostofi, “Co-Optimization of Communication and Motion Planning of a Robotic Operation under Resource Constraints and in Fading Environments,” *IEEE Transactions on Wireless Communications*, vol. 12, no. 4, pp. 1562–1572, 2013.
- [31] A. Muralidharan and Y. Mostofi, “Path Planning for a Connectivity Seeking Robot,” in *Proceedings of 2017 IEEE Globecom Workshops (GC Wkshps)*, 2017, pp. 1–6.
- [32] U. Ali, H. Cai, Y. Mostofi, and Y. Wardi, “Motion-Communication Co-Optimization With Cooperative Load Transfer in Mobile Robotics: An Optimal Control Perspective,” *IEEE Transactions on Control of Network Systems*, vol. 6, no. 2, pp. 621–632, 2019.
- [33] J. N. Twigg, J. R. Fink, P. L. Yu, and B. M. Sadler, “Efficient base station connectivity area discovery,” *The International Journal of Robotics Research*, vol. 32, no. 12, pp. 1398–1410, 2013.
- [34] S. Caccamo, R. Parasuraman, L. Freda, M. Gianni, and P. Ögren, “RCAMP: A resilient communication-aware motion planner for mobile robots with autonomous repair of wireless connectivity,” in *Proceedings of 2017 IEEE/RSJ International Conference on Intelligent Robots and Systems (IROS)*, 2017, pp. 2010–2017.
- [35] M. M. Zavlanos and G. J. Pappas, “Distributed Connectivity Control of Mobile Networks,” *IEEE Transactions on Robotics*, vol. 24, no. 6, pp. 1416–1428, 2008.
- [36] H. Yang, J. Zhang, S. Song, and K. B. Lataief, “Connectivity-Aware UAV Path Planning with Aerial Coverage Maps,” in *Proceedings of 2019 IEEE Wireless Communications and Networking Conference (WCNC)*, 2019, pp. 1–6.
- [37] L. Clark, J. Edlund, M. Net, T. Vaquero, and A. akbar Aghamohammadi, “PropEM-L: Radio Propagation Environment Modeling and Learning for Communication-Aware Multi-Robot Exploration,” in *Proceedings of Robotics: Science and Systems*, 2022.
- [38] Y. Yang, Y. Lyu, Y. Zhang, I. Gao, and W. Luo, “Integrating Online Learning and Connectivity Maintenance for Communication-Aware Multi-Robot Coordination,” in *Proceedings of 2024 IEEE/RSJ International Conference on Intelligent Robots and Systems (IROS)*, 2024, pp. 5770–5776.
- [39] Y. Kantaros and M. M. Zavlanos, “Distributed Intermittent Connectivity Control of Mobile Robot Networks,” *IEEE Transactions on Automatic Control*, vol. 62, no. 7, pp. 3109–3121, 2017.
- [40] Y. Kantaros, M. Guo, and M. M. Zavlanos, “Temporal Logic Task Planning and Intermittent Connectivity Control of Mobile Robot Networks,” *IEEE Transactions on Automatic Control*, vol. 64, no. 10, pp. 4105–4120, 2019.
- [41] G. Li, R. Han, S. Wang, F. Gao, Y. C. Eldar, and C. Xu, “Edge Accelerated Robot Navigation With Collaborative Motion Planning,” *IEEE/ASME Transactions on Mechatronics*, vol. 30, no. 2, pp. 1166–1178, 2025.
- [42] W. Hurst and Y. Mostofi, “Optimization of Mobile Robotic Relay Operation for Minimal Average Wait Time,” *IEEE Transactions on Wireless Communications*, vol. 22, no. 6, pp. 3733–3747, 2023.
- [43] M. S. Parwez, S. T. Srivillibhutturu, S. V. R. Kopparthi, A. Misba, D. Roy, H. Olufowobi, and C. Kim, “CTMap: LLM-Enabled Connectivity-Aware Path Planning in Millimeter-Wave Digital Twin Networks,” *arXiv preprint arXiv:2601.00110*, 2026.
- [44] L. Achey, B. Crockett, C. Heckman, and B. Hayes, “RF-Modulated Adaptive Communication Improves Multi-Agent Robotic Exploration,” *arXiv preprint arXiv:2602.12074*, 2026.
- [45] E. Psomiadis, D. Maity, and P. Tsiotras, “Communication-Aware Map Compression for Online Path-Planning,” in *Proceedings of 2024 IEEE International Conference on Robotics and Automation (ICRA)*, 2024, pp. 12 368–12 374.
- [46] J. Bi, Y. Wang, B. Yu, H. Cao, T. Shi, and L. Huang, “Supplementary open dataset for WiFi indoor localization based on received signal strength,” *Satellite Navigation*, vol. 3, no. 1, p. 25, 2022.
- [47] D. Ruan, S. Mozaffari, S. Adriaenssens, and A. Adel, “A Latency-Aware Framework for Visuomotor Policy Learning on Industrial Robots,” *arXiv preprint arXiv:2602.14255*, 2026.
- [48] M. Wei, C. Wan, J. Peng, X. Yu, Y. Yang, D. Feng, W. Cai, C. Zhu, T. Wang, J. Pang, and X. Liu, “Ground Slow, Move Fast: A Dual-System Foundation Model for Generalizable Vision-Language Navigation,” in *Proceedings of The 14th International Conference on Learning Representations (ICLR)*, 2026.